Electrostatic screening mediated by interfacial charge transfer in molecular assemblies on semiconductor substrates

A. Tan, S. R. Wagner,* and P. P. Zhang†
Department of Physics and Astronomy, Michigan State University, East Lansing, Michigan 48824-2320, USA
(Received 31 March 2017; revised manuscript received 21 June 2017; published 31 July 2017)

Using scanning tunneling microscopy and spectroscopy (STM, STS), we report the electronic structures of self-assembled zinc phthalocyanine (ZnPc) and hexadecafluorinated zinc phthalocyanine (F_{16}ZnPc) monolayers on the Si(111)-B surface. We show that interfacial charge transfer occurs in the F_{16}ZnPc monolayer, which gives rise to a pronounced spatial variation of the occupied molecular state across the molecular assembly, a feature not observed in the molecular states of the ZnPc overlayer without the presence of interfacial charge transfer. We attribute this observation to the inhomogeneous electrostatic screening of the intraorbital Coulomb interaction in molecular adsorbates arising from the substrate boron distribution. This study highlights the impact of the substrate electrostatic environment on molecular electronic structures, an essential aspect in the applications of organic and molecular electronic devices.

DOI: 10.1103/PhysRevB.96.035313

I. INTRODUCTION

Understanding and control of heterointerfaces between organic and inorganic materials are critical for the development of organic electronics, molecular electronics, molecular/biological sensors, and energy harvesting devices [1–6]. A central problem among various interfacial phenomena is the charge behavior. Charge transfer or charge redistribution can result in the formation of an interfacial dipole layer or band bending [1,7,8]. Interface states, defects, and disorders in organic materials, in addition, may act to pin the Fermi level of the hybrid system [1,9,10]. All these factors are crucial in determining the energy-level alignment at heterointerfaces, which ultimately impacts charge injection and collection in organic electronic devices.

What further complicates organic-inorganic heterointerfaces is that molecular electronic structures are often susceptible to polarization and electrostatic environments [11–15]. This is due to the weak intermolecular interaction and overlap of wave functions in organic semiconductors which tends to localize charge carriers. From a theoretical perspective, the localization of charges necessitates the consideration of charging energy (U) originating from the on-site Coulomb electron-electron interaction that is beyond the single-particle or mean-field description, as molecules are temporarily charged by the injection or extraction of electrons during electronic structure measurements. It is known that the energy of an N-electron molecule, with the consideration of U, can be approximated as $E_N = \sum_{i=1}^{N} (\varepsilon_i - \mu) + \frac{\Delta N(\Delta N-1)}{2} U$, where ΔN represents the net charge of the molecule, ε_i the mean-field molecular energy levels, and μ the chemical potential of the substrate that the molecule adsorbs on. The charging energy can be attenuated by a variety of factors such as substrate screening and polarization of neighboring molecules, resulting in a molecular electronic structure that is highly susceptible to the electrostatic environment and molecular packing [5,16–19]. Moreover, the frontier molecular energy levels that are relevant to device operation, i.e., the highest occupied molecular orbital (HOMO) and the lowest unoccupied molecular orbital (LUMO), could also be altered by the orientation of molecules within the film owing to the quadrupole field that shifts the local vacuum level outside the molecular layer [5,14,20–22].

Thus far, most of the studies on molecular electronic structures and interfacial properties have been conducted on metallic and insulating substrates. However, due to the need for integrating organic semiconductors with their inorganic counterparts in modern device architectures, it is imperative to explore the growth of organic thin films on inorganic semiconductors and to establish a comprehensive understanding of the electronic structure and energy-level alignment at the associated heterointerfaces. A notable challenge along this line of research is that the prevalence of surface states on inorganic semiconductors, such as Si, typically results in the formation of covalent bonds with molecular adsorbates, which hinders molecular diffusion and self-assembly [23]. To address this issue, methodologies for passivating or deactivating the surface states have been developed.

Recently, it has been shown that the growth of molecular structures can be facilitated on the Si(111)-B $\sqrt{3} \times \sqrt{3}$ surface where free radicals in the surface dangling bonds are depleted by the trivalent boron atoms segregated in the third atomic layer [24–27]. Furthermore, owing to the low defect density of the surface, the anisotropic step-flow growth of metal phthalocyanine, which exhibits long-range molecular ordering in both in-plane and out-of-plane directions, has been demonstrated [28–32]. Despite these initial successes in the molecular growth, molecular electronic structures and interfacial energy-level alignment have not been well studied in this system. It is important to note that the deactivation process which creates the Si(111)-B $\sqrt{3} \times \sqrt{3}$ surface could result in an inhomogeneous subsurface boron distribution beyond the third atomic layer, potentially influencing the electrostatic environment and thus the electronic structure of the molecular overlayer [33]. However, these effects cannot be well isolated in ensemble-averaged electronic structure measurements such as ultraviolet photoemission spectroscopy

*Present address: General Motors Research and Development, Warren, MI 48090, USA.
†Corresponding author: zhang@pa.msu.edu

 ©2017 American Physical Society

(UPS) or x-ray photoemission spectroscopy (XPS). Thus, local probe techniques that can simultaneously resolve the molecular ordering and electronic structures are necessary.

In this work, using scanning tunneling microscopy and spectroscopy (STM/STS), we show that zinc phthalocyanine (ZnPc) and hexadecafluorinated zinc phthalocyanine (F_{16}ZnPc) both form ordered self-assemblies on the Si(111)-B $\sqrt{3} \times \sqrt{3}$ surface, with the latter inducing a downward band bending in the bulk Si which is indicative of electron transfer from the F_{16}ZnPc molecules to the substrate. This charge transfer is further accompanied by pronounced energy-level variations of an occupied molecular state across the F_{16}ZnPc assembly, not observed for the unoccupied molecular orbital of F_{16}ZnPc nor in the molecular states of the ZnPc overlayer which does not undergo any charge transfer with the substrate. We attribute this observation to the inhomogeneous electrostatic screening of the intraorbital Coulomb interaction in molecular adsorbates arising from the substrate boron distribution. This mechanism impacts only the molecular orbital that is directly involved in the interfacial charge-transfer process.

II. EXPERIMENTAL METHODS

Experiments were carried out in an ultrahigh vacuum (UHV) setup using a commercial LT-Omicron scanning microscope operated at 77 K. STM images were taken at constant current mode with a tungsten tip. STS acquisition was achieved with the lock-in technique at a constant tip-sample distance controlled by the voltage (V_s) and current (I_t) set points before the feedback loop is disabled. Typical modulation bias and frequency were 26 mV and 1 kHz, respectively. Spectra on Ag(111) were taken periodically as a reference to confirm tip consistency. In order to prepare the Si (111)-B $\sqrt{3} \times \sqrt{3}$ surface, we used degenerately boron-doped Si(111) wafers with a resistivity of 0.01−0.001 Ω cm. The substrate was first cleaned via RCA1 and RCA2 procedures before it was loaded into the UHV environment for thermal treatment. The sample was annealed by direct heating with repeated flash annealing at 1200 °C, followed by an hour of annealing at 800 °C to induce boron segregation on the third atomic layer. ZnPc and F_{16}ZnPc were purified by sublimation processing before being loaded into the UHV system. The molecules were then degassed prior to use. ZnPc and F_{16}ZnPc monolayers were grown by thermal evaporation with the substrate held at room temperature and 110 °C, respectively.

III. RESULTS

A. Topography and geometric structure of molecular overlayers

In the following discussion, the Si(111)-B $\sqrt{3} \times \sqrt{3}$ surface is abbreviated as Si(111)-B. Figure 1 shows the STM topography images of the Si(111)-B surface and the ZnPc and F_{16}ZnPc overlayers grown on this supporting substrate. As illustrated in Figs. 1(a) and 1(b), the atomically smooth Si(111)-B surface is formed by the segregation of boron atoms in the third atomic layer which substitutes Si at the S_5 sites [34]. During this process, the trivalent boron atoms deplete electrons from the dangling bonds of the topmost Si adatoms, leading to a deactivated surface with a large surface band gap as displayed in Fig. 2(a). The chemical inertness and atomic flatness of the surface make Si(111)-B an ideal template for exploring the formation of organized organic molecular assemblies on inorganic substrates.

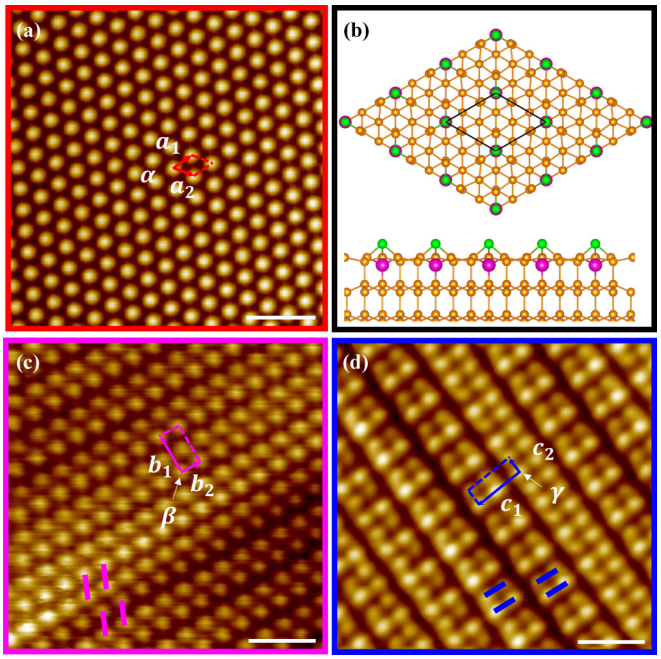

FIG. 1. STM topography images of (a) Si(111)-B ($V_s = 2$ V, $I_t = 5$ pA), (c) ZnPc ($V_s = 1.8$ V, $I_t = 60$ pA), and (d) F_{16}ZnPc ($V_s = 2$ V, $I_t = 5$ pA) taken at 77 K. Scale bars represent 2 nm. Lattice parameters of the three unit cells are given by (a) $a_1 = a_2 = 0.665 \pm 0.005$ nm, $\alpha = 60°$; (c) $b_1 = 1.23 \pm 0.01$ nm, $b_2 = 0.67 \pm 0.01$ nm, $\beta = 92 \pm 1°$; and (d) $c_1 = 1.56 \pm 0.02$ nm, $c_2 = 0.58 \pm 0.01$ nm, $\gamma = 89 \pm 1°$. (b) Schematics of Si(111)-B in the top view (top) and side view (bottom), adapted from Ref. [30]. The free radicals in the Si adatoms are deactivated by boron atoms located on the 3rd atomic layer directly beneath the adatoms.

Self-assembly of ZnPc and F_{16}ZnPc molecular adsorbates into monolayers with well-defined epitaxial registration to the Si(111)-B substrate is guided by the delicate balance between the molecule-molecule and molecule-substrate interactions [28,29]. As shown in Fig. S1 [35], both assemblies adopt a tilted molecular configuration. This is due to the corrugated surface potential landscape of Si(111)-B, originating from the relatively large lattice constant of the surface, as well as the comparable strength of the molecule-molecule and molecule-substrate binding energies, leading to the molecules sacrificing a portion of the surface adsorption energy to maximize the $\pi - \pi$ intermolecular interaction with increasing molecular coverage [30]. Furthermore, geometric structures, as illustrated in Fig. S1, reveal that the ZnPc overlayer adopts an incommensurate epitaxial registration to the Si(111)-B surface, while F_{16}ZnPc forms a point-on-line coincident structure. The distinct epitaxial relationship between the molecular overlayers and the substrate surface gives rise to the contrast variation observed in the STM topography images (Figs. 1(c), 1(d), and Fig. S1 [30]). Lastly, as discussed earlier, molecular electronic structures are sensitive to their electrostatic environment. The uniform molecular packing and

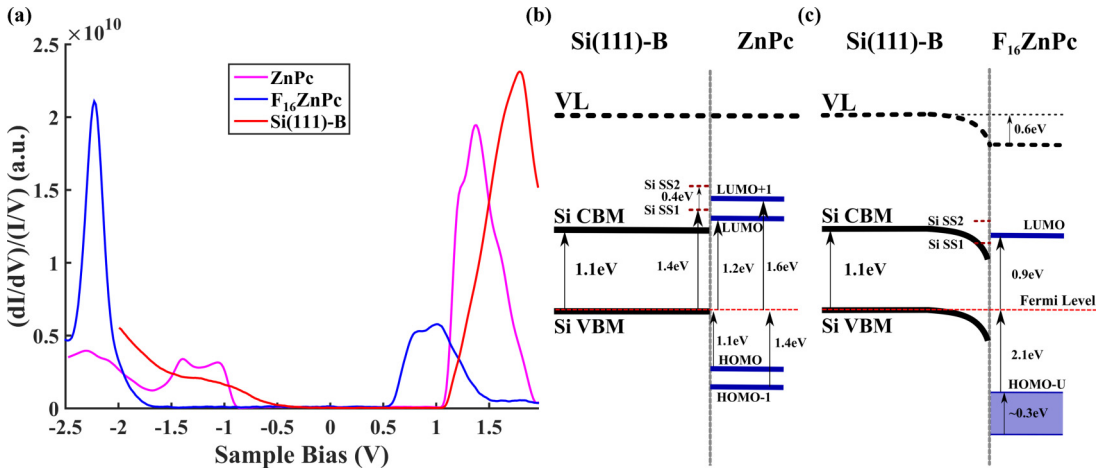

FIG. 2. (a) STS data taken on Si(111)-B (set point: $V_s = -2$ V, $I_t = 100$ pA, red), ZnPc molecular overlayer ($V_s = -2$ V, $I_t = 100$ pA, magenta) and F_{16}ZnPc molecular overlayer ($V_s = 2$ V, $I_t = 50$ pA, blue). Energy-band diagrams illustrated for (b) Si(111)-B/ZnPc and (c) Si(111)-B/F_{16}ZnPc. Energy levels are defined by STS peaks unless specified. For simplicity, it is assumed that there is no interface dipole so that the vacuum level is continuous at the F_{16}ZnPc/Si(111)-B heterointerface. The energy range (~0.3 eV) of the occupied molecular orbital of the F_{16}ZnPc overlayer, as provided in (c), is derived based on the analysis of Fig. 3(b).

molecular orientation realized for both the ZnPc and F_{16}ZnPc structures on the Si(111)-B surface thus uniquely allow for the disentanglement of the electrostatic effect of the substrate from that of the neighboring molecules.

B. STS of deactivated Si surface

Figure 2(a) shows the characteristic STS curves taken on the ZnPc monolayer, the F_{16}ZnPc monolayer, and the Si(111)-B supporting substrate with colors corresponding to the outlines of the images shown in Fig. 1. To understand the STS curves and the associated molecular electronic features, we first look into the band structure of the Si(111)-B surface. The dangling bond deactivation process leads to the formation of two unoccupied surface states, SS1 and SS2, as well as occupied surface states that originate from the Si(adatom)-Si(second layer) and Si(second layer)-B(third layer) backbonds [33,36–39]. These backbond states are positioned at least 0.56 eV below the valence band maximum (at the Γ point), depending on the location in k space [37]. Thus, due to the overlap between the occupied surface states and the Si bulk valence states, the precise rise of the filled density of states is extremely sensitive to the STS set points and consequently the tip-sample distance. For instance, at a large tip-sample distance (controlled by the voltage and current set points before the STM feedback is disabled), we see a rise of the filled DOS at ~0.5 V [Fig. 2(a)], suggesting that the surface states are the primary contributing factor to the STS spectra. However, when the tip-sample distance is small, the DOS of the bulk Si valence band becomes the predominant factor, causing the DOS to rise near the Fermi level, as shown in Fig. 4(c). This is expected for the degenerately boron-doped Si sample. It is important to note, however, that the small tip-sample distance as established in Fig. 4(c) is experimentally difficult to realize in molecular assembly studies. Because of the low electrical conductivity of the molecular overlayer, a relatively large tip-sample distance has to be utilized to prevent any damage to the molecular structures and the tip.

On the positive side of the spectrum, in contrast, we observe an overall consistent rise of the DOS features regardless of the tip-sample distance [Fig. 2(a) vs Fig. 4(c)]. To address the nature of these states, we first take a close look at the band structure calculated by density functional theory (DFT) [37]. It shows that SS1 is the lowest lying state around the Γ point, followed by the SS2 state, which is convoluted with the bulk conduction band. Since the effective tunneling decay constant, $\kappa = \sqrt{(\frac{2m_e\Phi_b}{\hbar^2} + k_{||}^2)}$, is a function of the parallel momentum, it is expected that the larger the $k_{||}$, the weaker its contribution to the overall tunneling spectra [40,41]. Note that m_e is the electron mass and Φ_b the tunneling barrier. Therefore, although the bulk states will be probed at a small tip-sample distance as we have discussed earlier, we still observe the rise of SS1 first, owing to the much stronger tunneling into the states around the Γ point where $k_{||}$ is minimum. This results in no noticeable change in the rise of the empty states between Figs. 2(a) and 4(c). Furthermore, Gaussian fitting of the spectral feature (see Fig. S2 [35]) suggests that the SS1 and SS2 states are centered at ~1.4 V and ~1.8 V, respectively, which is consistent with the previous report [36].

C. Electronic structures of molecular assemblies

When molecules are deposited on the Si(111)-B surface, however, electrons will tunnel into the molecular overlayer first then into the supporting substrate during the STM/STS measurements. Provided the surface states of the underlying Si(111)-B can be probed through the molecular layer, they will serve as the reference during the analysis of interfacial band alignment as the energy levels of these states are fixed relative to the band edges of the bulk Si. For the ZnPc spectrum displayed in Fig. 2(a), Gaussian analysis reveals four distinct peaks which altogether construct the main DOS feature at positive sample bias (see Fig. S2). The locations of these unoccupied density-of-state peaks are summarized in Table I. Specifically, those located at 1.37 ± 0.04 V and 1.81 ± 0.04 V align with the SS1 and SS2 surface states of the bare Si(111)-B substrate, suggesting that the

TABLE I. Averaged Gaussian-fit peak positions of the unoccupied density-of-state features in the STS spectra taken on ZnPc, F_{16}ZnPc, and Si(111)-B, respectively. Error bars are derived from the standard deviation of peak positions from multiple data sets, taking the lock-in modulation voltage (26 meV) as the lower bound. Dashes represent the absence of Gaussian peaks that can be resolved in the fitting presented in Fig. S2.

Material	Molecular peak (V)	Si SS1 (V)	Molecular peak (V)	Si SS2 (V)
ZnPc	1.20 ± 0.03	1.37 ± 0.04	1.59 ± 0.06	1.81 ± 0.04
F_{16}ZnPc	–	0.73 ± 0.03	0.94 ± 0.03	1.16 ± 0.05
Si(111)-B	–	1.40 ± 0.04	–	1.79 ± 0.03

adsorption of the ZnPc overlayer does not noticeably disturb the charge distribution in the substrate. This is consistent with earlier DFT calculations, which demonstrates a negligible charge transfer and/or charge redistribution between ZnPc and Si(111)-B [30]. Therefore, the ZnPc/Si(111)-B heterointerface is anticipated to follow vacuum-level alignment, as depicted in Fig. 2(b). Additionally, with the aid of differential conductance (dI/dV) mapping, capable of revealing the spatial distribution of the density of states, we attribute the other two peaks, centered at 1.20 ± 0.03 V and 1.59 ± 0.06 V, to the LUMO and LUMO + 1 of the ZnPc molecular overlayer, respectively. The dI/dV map of the LUMO + 1 molecular orbital is illustrated in the inset of Fig. 3(a), which shows distinctly different features from the DOS distribution of the SS1 and SS2 surface states (see Fig. S5 for more details [35]). The asymmetric appearance of the molecular lobes in each individual ZnPc molecule is likely a result of degeneracy lifting of the molecular orbitals, resulting in a C4 to C2 symmetry reduction [42–45]. Note that due to the tilted molecular configuration where only the top two pyrrolelike rings are visualized, we do not expect to observe the nodal planes in the dI/dV map as for the flat-lying molecules.

Regarding the F_{16}ZnPc spectrum, the entire STS curve appears to shift towards more negative energies (sample biases) in comparison to spectra collected on the ZnPc or the bare Si(111)-B surface. Similar to the previous discussion, we can apply a Gaussian analysis to deconstruct the unoccupied DOS feature residing within the Si(111)-B surface gap. Among the three Gaussian-fit peaks centered at 0.73 ± 0.03 V, 0.94 ± 0.03 V, and 1.16 ± 0.05 V, peaks 1 and 3 share the same separation in energy, within experimental error, as that observed between the SS1 and SS2 states of the bare Si(111)-B surface. If we assume that these two peaks are indeed associated with the surface states of the substrate, their shift towards the Fermi level (~0.6 eV) provides direct evidence of downward band bending in the bulk Si, as illustrated in Fig. 2(c). Electron transfer from F_{16}ZnPc molecules to the Si substrate is anticipated to be the origin of this band bending. It is worth pointing out that the Fermi level (at zero sample bias in the STS spectra) represents the charge equilibrium of the entire system and therefore is determined by the bulk Si regardless of molecular adsorption on the surface. Lastly, the electron density distribution of peak 2, as revealed in the dI/dV map [inset of Fig. 3(b)], displays an alternating contrast along the F_{16}ZnPc molecular stripes, very much like the topography of the overlayer (see detailed structural analysis in Fig. S1). This suggests that peak 2 corresponds to a molecular orbital, and the distinctive molecular registration to the Si(111)-B surface gives rise to the observed contrast in the dI/dV map [29].

Thus far, our discussion has been concentrated on the band-structure analysis guided by the SS1 and SS2 states of the Si(111)-B surface. Next, we will examine how the differentiating interfacial charge-transfer behavior between ZnPc/Si(111)-B and F_{16}ZnPc/Si(111)-B impacts the occupied

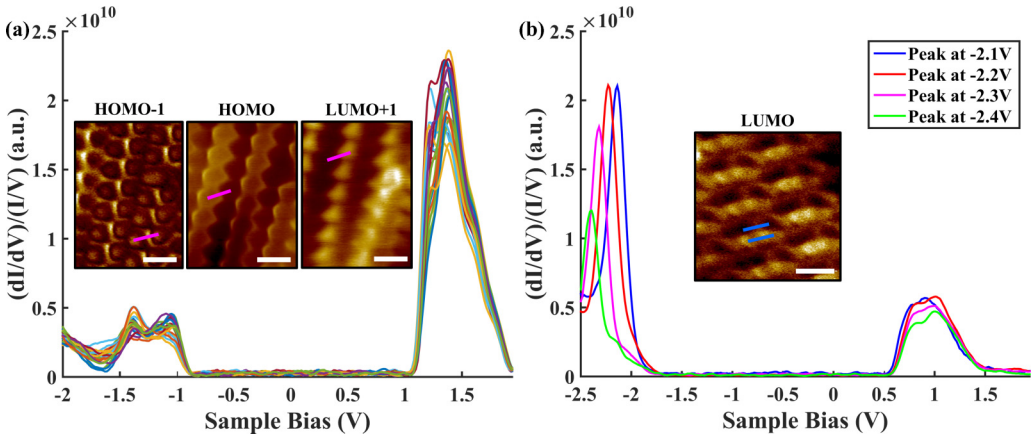

FIG. 3. (a) Multiple STS spectra (set point: −2 V, 100 pA) taken at various locations on the ZnPc overlayer. No peak variation is observed among the curves. The positive DOS feature is a convolution of the LUMO, LUMO + 1, and Si surface states. The two well-resolved occupied molecular states are located at ~ − 1.4 V and −1.1 V. Inset: dI/dV map of ZnPc obtained at (I_t = 100 pA): −1.5 V (left), −1 V (middle), 1.4 V (right). Magenta lines denote individual ZnPc molecules. (b) Four characteristic STS spectra (set point: 2 V, 50 pA) taken at multiple locations on the F_{16}ZnPc overlayer. The positive DOS feature that remains consistent (centered at ~1 V) is a convolution of the Si surface states and molecular LUMO. The occupied molecular orbital observed on the negative sample bias, however, is shifted in energy position. Inset: dI/dV map of F_{16}ZnPc at 1 V, 50 pA. Blue lines denote individual F_{16}ZnPc molecules. Scale bars represent 1 nm.

molecular states. The inset of Fig. 3(a) shows the dI/dV maps of ZnPc taken at −1.0 V and −1.5 V, which illustrate asymmetric molecular features similar to those observed for the dI/dV map associated with LUMO + 1. Figure 3(a) also illustrates the overlay of STS curves taken on multiple locations of the ZnPc overlayer. Highly consistent features are observed with the DOS peaks overlapping in energy positions and only differing slightly in intensity. Intriguingly, when curves taken on the F_{16}ZnPc overlayer are put together, significant peak position variation as large as several hundred meV can be identified for the occupied molecular orbital at negative sample bias, whereas the empty states, e.g., LUMO, SS1, and SS2, remain fixed [Fig. 3(b)]. More examples of this phenomenon can be found in Fig. S3 [35]. It is worth mentioning that the STS curves are taken in areas away from the assembly edges to prevent the disturbance of the local electrostatic environment by the reduced molecular coordination at the edges [16].

A natural question that arises is how to account for the spatial variation of the occupied molecular level in the F_{16}ZnPc monolayer which is not observed for its LUMO state or in the molecular states of the ZnPc layer. As discussed earlier, the electronic structure of organic molecular thin films can be modulated by the molecular orientation, packing, or local ordering [5,14,20–22]. However, as shown in the STM images (Fig. 1) as well as in an earlier study [29], F_{16}ZnPc molecules are packed uniformly with a universal tilted orientation in the overlayer. Molecular orbital levels may also move relative to the substrate Fermi level by the formation of an interface dipole [1,6]. Nevertheless, if this would be the case, HOMO and LUMO should shift rigidly together, which is different from what has been observed in the STS spectra in Fig. 3(b).

D. Inhomogeneous substrate screening

Another potential contribution to the tailoring of the molecular electronic structure is electrostatic screening from the substrate [16–19]. The thermal annealing process for creating the deactivated Si(111)-B surface inevitably introduces an inhomogeneous distribution of boron substituents in the bulk. Since the dielectric constant varies with doping concentration in degenerately doped Si [46,47], the subsurface boron inhomogeneity can result in a modulated local electrostatic environment for molecular adsorbates, which may consequently influence their electronic structures. To illustrate this correlation, we first explore the spatial variation of the subsurface boron distribution in the Si(111)-B substrate. Although STM is a surface-sensitive technique, imaging of subsurface dopants is feasible, especially when the surface states lie in energies that do not mask the bulk dopant states [33,48–50].

Figures 4(a) and 4(b) display the STM topography image of the Si(111)-B surface taken at -0.1 V and 1.3 V, respectively. Hillocks, as indicated by the red arrow, are observed in the filled-state image, which correspond to the more or less dimmer areas in the empty-state image. To explain this contrast that is likely related to the boron distribution in the bulk, we further perform site-specific STS [Fig. 4(c)] at a small tip-sample distance (set point: $V_s = -0.5$ V, $I_t = 300$ pA) where the tunneling current is more sensitive to the bulk states. The STS taken on the hillock in Fig. 4(a) displays an earlier rise of the filled state and a later rise of the empty state with respect to the Fermi level, in comparison to the spectrum obtained on the dark area (blue arrow). This phenomenon is expected to arise from the Coulomb potential of the thermally ionized boron dopants which inhibit/enhance the downwards/upwards tip-induced band bending during the filled/empty-state tunneling, as illustrated in the inset of Fig. 4(c). Consequently, areas with higher concentration of subsurface boron will appear brighter in the filled-state images due to the larger integrated density of states, and vice versa. Since the Coulomb potential $V = \frac{q}{4\pi\varepsilon_0\varepsilon r} e^{-r/r_s}$ (r_s is screening length within the bulk) is attenuated rapidly by the screening factor in degenerately doped Si [51], the hillocks are expected to correspond to boron atoms near the surface, e.g., in the fourth atomic layer, which will spread into more extended but less protruding regions when boron atoms are positioned in deeper layers. It should also be noted that due to the screening effect the magnitude of the band bending modulated by the Coulomb potential is rather small (see detailed analysis in Fig. S4 [35]), which falls within the uncertainty of the Gaussian fits as listed in Table I. As a result, when the STS curves are

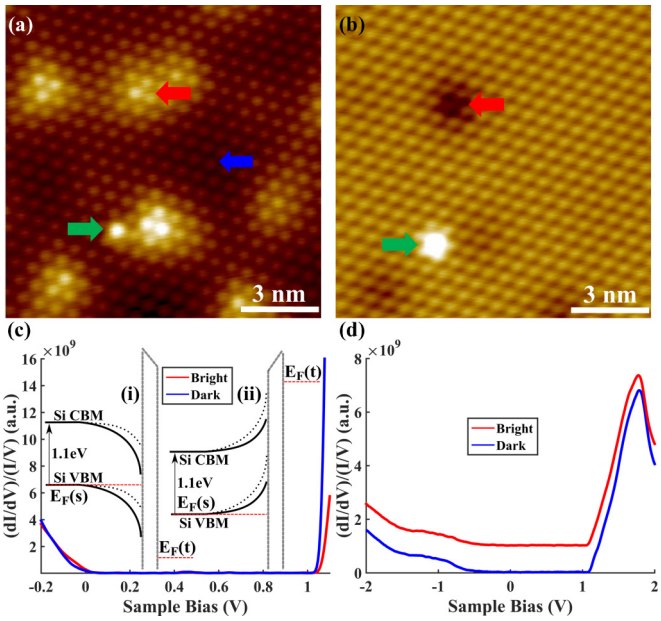

FIG. 4. STM topography images of Si(111)-B obtained at 77 K at (a) $V_s = -0.1$ V, $I_t = 100$ pA and (b) $V_s = 1.3$ V, $I_t = 300$ pA. Subsurface boron dopant (beyond the 3rd atomic layer) and surface dangling bond defect are indicated by the red and green arrows, respectively. The blue arrow points to a region with a low concentration of subsurface boron. (c) Averaged STS spectra taken at $V_s = -0.5$ V, $I_t = 300$ pA on the bright and dark regions indicated by the red and blue arrows in (a), respectively. Insets (i) and (ii) illustrate the tip-induced band bending modulated by the Coulomb potential of thermally ionized boron dopants under the filled-state and empty-state tunneling conditions, respectively, where the dotted line in the schematics refers to the band structure on the bright areas (hillocks) with accumulated subsurface boron and the solid line refers to the dark areas where the boron accumulation is minimal. (d) STS taken at $V_s = -2$ V, $I_t = 100$ pA on bright (red) and dark (blue) areas as indicated by colored arrows in (a). The curves are vertically offset for clarity, and there is no noticeable modulation on the apparent band gap or density-of-states features.

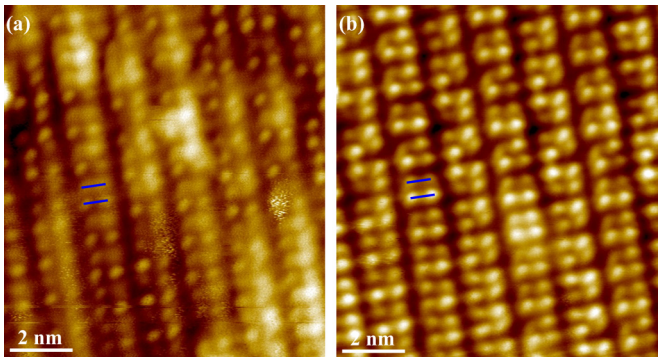

FIG. 5. STM topography images of F_{16}ZnPc obtained at 77 K at (a) $V_s = -2.5$ V, $I_t = 1$ pA and (b) $V_s = 2$ V, $I_t = 5$ pA. Significant contrast variation is observed in the filled-state image across the molecular structure, which is likely correlated to the subsurface boron inhomogeneity observed in Fig. 4(a). Uniform features are observed in the empty-state image, although small-scale contrast variation, resulting from the epitaxial registration between the molecular assembly and the underlying Si lattice, can be identified from molecule to molecule. Blue bars represent individual F_{16}ZnPc molecules.

taken on the Si(111)-B surface at a large tip-sample distance and over a wide voltage span, no noticeable modulation on the apparent band gap or DOS features can be identified between the boron-rich and -deficient areas, as shown in Fig. 4(d).

In order to visualize the spatial variation of the occupied molecular level in the F_{16}ZnPc overlayer, we image the F_{16}ZnPc/Si(111)-B surface at -2.5 V. As shown in Fig. 5(a), well-pronounced inhomogeneity is observed. This is strikingly different from the uniform features presented in the STM topography image of the same area at a positive sample bias shown in Fig. 5(b), suggesting that the contrast observed in Fig. 5(a) is electronic in nature. We speculate that the inhomogeneous electrostatic screening from the Si(111)-B substrate is the origin of this phenomenon, as evidenced by the comparable length scale of the contrast variation between the filled-state images of the F_{16}ZnPc overlayer and the bare Si(111)-B surface (see Fig. S6 [35]). Nevertheless, there is still one question that needs to be addressed. As depicted in Fig. 3, the peak variation is neither observed in the LUMO of F_{16}ZnPc nor in the molecular states of the ZnPc overlayer, which does not establish any charge transfer with the substrate. In order to reveal the underlying mechanism as to why the substrate screening impacts only the molecular orbital that is directly involved in the interfacial charge-transfer process, a more thorough discussion of the charge-transfer mechanism is required.

IV. DISCUSSION

The interaction between metal phthalocyanine (MPc) and inorganic substrate can be mediated by the central transition-metal ion, which is typically very strong when the metal center possesses a singly occupied d_z^2 orbital that can easily hybridize with protruding substrate orbitals such as Ag-sp_z states or the p_z states of Si adatoms on Si(111)-B [30,52]. Studies of the growth of CoPc on the Si(111)-B surface show that this strong interaction leads to flat-lying molecules with limited assembly sizes. Owing to the fully filled d-orbitals associated with the Zn center, the formation of strong chemical bonds between molecule and substrate is prohibited in Zn-based Pc molecules, as evidenced by the ability of ZnPc and F_{16}ZnPc to form long-range ordered structures on the Si(111)-B surface. Note that the F_{16}ZnPc overlayer displays a better epitaxial registration to the surface (point-on-line coincident in comparison to incommensurate for the case of ZnPc) as a result of the additional electrostatic interaction due to interfacial charge transfer [28–32]. Nevertheless, the electronic characterization of the F_{16}ZnPc overlayer has shown no indication of orbital hybridization, such as the formation of interface states [42,52–54]. This leads us to conclude that F_{16}ZnPc on Si(111)-B can be characterized as a weakly interacting system, which is fundamentally different from a chemisorption scenario.

In weakly interacting systems, electrons tunnel in integer amounts between frontier molecular orbitals and the substrate states, typically described by the integer charge transfer (ICT) model [3,53,55]. As the excess charge originating from the interfacial charge transfer results in the partial occupation of the specific molecular orbital involved in the ICT process, additional tunneling into this orbital, either by the extraction or injection of an electron, will lead to the splitting of the orbital into the singly occupied molecular orbital (SOMO), below the Fermi level, and the singly unoccupied molecular orbital (SUMO), above the Fermi level. The SOMO and SUMO are energetically separated by U associated with the intraorbital Coulomb repulsion (see schematics in Fig. S8) [19,35,52,55–59]. It should be noted that the intraorbital Coulomb repulsion will be necessarily larger than the intramolecular charging energy due to the more localized interaction between the incoming charge and the electron already present in the orbital. In the F_{16}ZnPc/Si(111)-B system, specifically, the HOMO orbital is involved in the interfacial charge transfer; thus it is expected to be split into SOMO/SUMO, which can also be described as HOMO-U/HOMO, respectively. The spatial variation of the SOMO/HOMO-U peak that is observed at negative sample bias seems correlated to the inhomogeneous screening effect from the subsurface boron distribution, whereas the SUMO/HOMO is likely positioned within the Si band gap, which prevents its observation due to the lack of resonant tunneling [60,61].

As has been described before, the charging energy U will be attenuated by a variety of factors such as the substrate screening and polarization of neighboring molecules. The substrate screening effect on the reduction of U can be estimated by the classical image-charge model $(qq')(\frac{1}{4\pi\varepsilon_0 \times 2(d-z_0)})$, where d is the molecule-substrate distance, $q' = q(\varepsilon - 1)/(\varepsilon + 1)$ is the effective image charge, and z_0 the effective position of the image plane [16,62]. Note that the latter two are both substrate dependent. In our system, areas of higher subsurface boron density are likely correlated to a more protruding image plane [63], resulting in a greater screening effect on the intraorbital Coulomb interaction which moves the SOMO/HOMO-U peak closer to the Fermi level (see Fig. S7 [35]). However, this inhomogeneous substrate screening should also perturb the intramolecular charging energy and thus the apparent band gap of the molecular overlayer, which seems contradictory to the experimental observation of the stationary position of the F_{16}ZnPc LUMO as well as the unperturbed ZnPc band gap.

To address this issue, it is worth noting that the probing of SOMO/HOMO-U changes the charge state of the F_{16}ZnPc molecule from +1 to +2, while the measurements of the ZnPc molecular levels and F_{16}ZnPc's own LUMO should involve the transition of the molecular charge states from 0 to ±1, and +1 to 0, respectively. Thus the screening modulation from the inhomogeneous subsurface boron distribution is expected to be weaker in the latter two cases due to the smaller change on the charge prefactor, associated with the orbital probing process, in the image-charge equation. In addition, the polarization response of molecular adsorbates to the image-charge field is expected to reduce the magnitude of the substrate screening [62]. The more delocalized nature of the F_{16}ZnPc LUMO and ZnPc molecular orbitals will result in a greater polarizability [64–68] as compared to the F_{16}ZnPc HOMO, leading to a larger reduction in the substrate screening. We speculate that the combination of these two effects is responsible for the experimental observation where the SOMO/HOMO-U of F_{16}ZnPc is the only energetically varied orbital across the molecular overlayers. Nevertheless, the precise determination of location-dependent q', z_o, as well as the polarization response which collectively impacts the screening reduction on U will require extensive theoretical investigations in the future [13,62,69,70].

V. CONCLUSION AND PROSPECTS

In conclusion, we have demonstrated that F_{16}ZnPc molecular assemblies exhibit charge transfer with the Si(111)-B substrate, as corroborated by the downward band bending in the bulk Si. When the electronic structures of the F_{16}ZnPc and ZnPc monolayers are compared, a noticeable variation in the energy level of the occupied molecular orbital is observed across the F_{16}ZnPc overlayer, which is in sharp contrast to the constant energy levels of the ZnPc orbitals and F_{16}ZnPc's own LUMO. This is hypothesized to originate from the subsurface boron distribution in the Si(111)-B substrate, which causes an inhomogeneous electrostatic screening of the intraorbital Coulomb interaction in F_{16}ZnPc due to the partially filled HOMO resulting from the interfacial charge-transfer process.

In terms of integrating organic molecular systems with mainstream inorganic semiconductors in device architectures, this observation puts a strong emphasis on the homogeneity of semiconducting substrates. Although molecular thin films can be grown into long-range ordered structures with a high crystallinity on Si(111)-B owing to the deactivated surface with low defect density, variations in the subsurface dopant concentration, even a few atomic layers deep, can have a drastic impact on the molecular electronic structures and consequently the charge injection/collection behaviors that are of paramount importance to the operation of organic and molecular electronic devices.

ACKNOWLEDGMENTS

We acknowledge financial support from the U.S. Department of Energy (DOE), Office of Science Early Career Research Program (Grant No. DE-SC0006400), through the Office of Basic Energy Sciences. We also acknowledge R. R. Lunt for his help with the sublimation process to purify the molecules used in this study.

[1] J. Hwang, A. Wan, and A. Kahn, Mater. Sci. Eng. R-Reports **64**, 1 (2009).
[2] D. Cahen, A. Kahn, and E. Umbach, Mater. Today **8**, 32 (2005).
[3] S. Braun, W. R. Salaneck, and M. Fahlman, Adv. Mater. **21**, 1450 (2009).
[4] S. Braun, W. Osikowicz, Y. Wang, and W. R. Salaneck, Org. Electron. **8**, 14 (2007).
[5] F. Bussolotti, J. Yang, A. Hinderhofer, Y. Huang, W. Chen, S. Kera, A. T. S. Wee, and N. Ueno, Phys. Rev. B **89**, 115319 (2014).
[6] H. Ishii, K. Sugiyama, E. Ito, and K. Seki, Adv. Mater. **11**, 605 (1999).
[7] H. Ishii, N. Hayashi, E. Ito, Y. Washizu, K. Sugi, Y. Kimura, M. Niwano, Y. Ouchi, and K. Seki, Phys. Status Solidi A **201**, 1075 (2004).
[8] I. Lange, J. C. Blakesley, J. Frisch, A. Vollmer, N. Koch, and D. Neher, Phys. Rev. Lett. **106**, 216402 (2011).
[9] S. Zhong, J. Q. Zhong, H. Y. Mao, J. L. Zhang, J. D. Lin, and W. Chen, Phys. Chem. Chem. Phys. **14**, 14127 (2012).
[10] M. Oehzelt, N. Koch, and G. Heimel, Nat. Commun. **5**, 4174 (2014).
[11] I. Avilov, V. Geskin, and J. Cornil, Adv. Funct. Mater. **19**, 624 (2009).
[12] M. Linares, D. Beljonne, J. Cornil, K. Lancaster, J. L. Bredas, S. Verlaak, A. Mityashin, P. Heremans, A. Fuchs, C. Lennartz, J. Ide, R. Mereau, P. Aurel, L. Ducasse, and F. Castet, J. Phys. Chem. C **114**, 3215 (2010).
[13] J. B. Neaton, M. S. Hybertsen, and S. G. Louie, Phys. Rev. Lett. **97**, 216405 (2006).
[14] S. Verlaak, D. Beljonne, D. Cheyns, C. Rolin, M. Linares, F. Castet, J. Cornil, and P. Heremans, Adv. Func. Mater. **19**, 3809 (2009).
[15] S. R. Yost, L. P. Wang, and T. Van Voorhis, J. Phys. Chem. C **115**, 14431 (2011).
[16] I. Fernández Torrente, K. J. Franke, and J. Ignacio Pascual, J. Phys.: Condens. Matter **20**, 184001 (2008).
[17] X. Lu, M. Grobis, K. H. Khoo, S. G. Louie, and M. F. Crommie, Phys. Rev. B **70**, 115418 (2004).
[18] J. D. Sau, J. B. Neaton, H. J. Choi, S. G. Louie, and M. L. Cohen, Phys. Rev. Lett. **101**, 026804 (2008).
[19] A. Mugarza, C. Krull, R. Robles, S. Stepanow, G. Ceballos, and P. Gambardella, Nat. Commun. **2**, 490 (2011).
[20] W. N. Han, K. Yonezawa, R. Makino, K. Kato, A. Hinderhofer, R. Murdey, R. Shiraishi, H. Yoshida, N. Sato, N. Ueno, and S. Kera, App. Phys. Lett. **103**, 253301 (2013).
[21] G. Heimel, I. Salzmann, S. Duhm, and N. Koch, Chem. Mater. **23**, 359 (2011).
[22] S. Duhm, G. Heimel, I. Salzmann, H. Glowatzki, R. L. Johnson, A. Vollmer, J. P. Rabe, and N. Koch, Nat. Mater. **7**, 326 (2008).

[23] N. Nicoara, Ó. Paz, J. Méndez, A. M. Baró, J. M. Soler, and J. M. Gómez-Rodríguez, Phys. Rev. B **82**, 075402 (2010).
[24] B. Baris, J. Jeannoutot, V. Luzet, F. Palmino, A. Rochefort, and F. Cherioux, ACS Nano **6**, 6905 (2012).
[25] Y. Makoudi, F. Palmino, M. Arab, E. Duverger, and F. Cherioux, J. Am. Chem. Soc. **130**, 6670 (2008).
[26] G. Copie, Y. Makoudi, C. Krzeminski, F. Cherioux, F. Palmino, S. Lamare, B. Grandidier, and F. Cleri, J. Phys. Chem. C **118**, 12817 (2014).
[27] B. Baris, V. Luzet, E. Duverger, P. Sonnet, F. Palmino, and F. Cherioux, Angew. Chem. Int. Ed. **50**, 4094 (2011).
[28] S. R. Wagner, R. R. Lunt, and P. Zhang, Phys. Rev. Lett. **110**, 086107 (2013).
[29] A. Tan, S. Wagner, and P. Zhang, J. Chem. Phys. **146**, 052809 (2017).
[30] S. R. Wagner, B. Huang, C. Park, J. Feng, M. Yoon, and P. Zhang, Phys. Rev. Lett. **115**, 096101 (2015).
[31] S. R. Wagner and P. P. Zhang, J. Phys. Chem. C **118**, 2194 (2014).
[32] S. R. Wagner and P. P. Zhang, Surf. Sci. **630**, 22 (2014).
[33] E. J. Spadafora, J. Berger, P. Mutombo, M. Telychko, M. Švec, Z. Majzik, A. B. McLean, and P. Jelínek, J. Phys. Chem. C **118**, 15744 (2014).
[34] I. W. Lyo, E. Kaxiras, and P. Avouris, Phys. Rev. Lett. **63**, 1261 (1989).
[35] See Supplemental Material at http://link.aps.org/supplemental/10.1103/PhysRevB.96.035313 for geometric simulations, Gaussian fits, and additional experimental data and analysis.
[36] C. Tournier-Colletta, B. Kierren, Y. Fagot-Revurat, and D. Malterre, Phys. Rev. B **87**, 075427 (2013).
[37] H. Q. Shi, M. W. Radny, and P. V. Smith, Phys. Rev. B **66**, 085329 (2002).
[38] A. B. McLean, L. J. Terminello, and F. J. Himpsel, Phys. Rev. B **41**, 7694 (1990).
[39] E. Kaxiras, K. C. Pandey, F. J. Himpsel, and R. M. Tromp, Phys. Rev. B **41**, 1262 (1990).
[40] J. Tersoff and D. R. Hamann, Phys. Rev. Lett. **50**, 1998 (1983).
[41] J. Tersoff and D. R. Hamann, Phys. Rev. B **31**, 805 (1985).
[42] M. Toader, T. G. Gopakumar, P. Shukrynau, and M. Hietschold, J. Phys. Chem. C **114**, 21548 (2010).
[43] W. H. Soe, C. Manzano, H. S. Wong, and C. Joachim, J. Phys.: Condens. Matter **24**, 354011 (2012).
[44] S.-H. Chang, S. Kuck, J. Brede, L. Lichtenstein, G. Hoffmann, and R. Wiesendanger, Phys. Rev. B **78**, 233409 (2008).
[45] T. Sonnleitner, I. Swart, N. Pavliček, A. Pöllmann, and J. Repp, Phys. Rev. Lett. **107**, 186103 (2011).
[46] M. H. Andrews, A. H. Marshak, and R. Shrivastava, J. Appl. Phys. **52**, 6783 (1981).
[47] S. Ristić, A. Prijić, and Z. Prijić, Serb. J. Electr. Eng. **1**, 237 (2004).
[48] R. M. Feenstra, J. M. Woodall, and G. D. Pettit, Phys. Rev. Lett. **71**, 1176 (1993).
[49] G. Mahieu, B. Grandidier, D. Deresmes, J. P. Nys, D. Stiévenard, and P. Ebert, Phys. Rev. Lett. **94**, 026407 (2005).
[50] L. Liu, J. Yu, and J. W. Lyding, Appl. Phys. Lett. **78**, 386 (2001).
[51] Y. D. Kwon, Phys. Rev. B **73**, 165210 (2006).
[52] A. Mugarza, R. Robles, C. Krull, R. Korytár, N. Lorente, and P. Gambardella, Phys. Rev. B **85**, 155437 (2012).
[53] M. Gruenewald, L. K. Schirra, P. Winget, M. Kozlik, P. F. Ndione, A. K. Sigdel, J. J. Berry, R. Forker, J.-L. Brédas, T. Fritz, and O. L. A. Monti, J. Phys. Chem. C **119**, 4865 (2015).
[54] A. Bendounan, F. Forster, A. Schöll, D. Batchelor, J. Ziroff, E. Umbach, and F. Reinert, Surf. Sci. **601**, 4013 (2007).
[55] O. T. Hofmann, P. Rinke, M. Scheffler, and G. Heimel, ACS Nano **9**, 5391 (2015).
[56] C. Krull, R. Robles, A. Mugarza, and P. Gambardella, Nat. Mater. **12**, 337 (2013).
[57] M. Hollerer, D. Luftner, P. Hurdax, T. Ules, S. Soubatch, F. S. Tautz, G. Koller, P. Puschnig, M. Sterrer, and M. G. Ramsey, ACS Nano **11**, 6252 (2017).
[58] J. Repp, G. Meyer, S. Paavilainen, F. E. Olsson, and M. Persson, Science **312**, 1196 (2006).
[59] K. A. Cochrane, A. Schiffrin, T. S. Roussy, M. Capsoni, and S. A. Burke, Nat. Commun. **6**, 8312 (2015).
[60] K. W. Hipps, D. E. Barlow, and U. Mazur, J. Phys. Chem. B **104**, 2444 (2000).
[61] M. Lackinger, T. Müller, T. G. Gopakumar, F. Müller, M. Hietschold, and G. W. Flynn, J. Phys. Chem. B **108**, 2279 (2004).
[62] P. Puschnig, P. Amiri, and C. Draxl, Phys. Rev. B **86**, 085107 (2012).
[63] S. Ossicini, C. M. Bertoni, and P. Gies, Europhys. Lett. **1**, 661 (1986).
[64] K. T. No, K. H. Cho, M. S. Jhon, and H. A. Scheraga, J. Am. Chem. Soc. **115**, 2005 (1993).
[65] J. Ren, S. Meng, Y. L. Wang, X. C. Ma, Q. K. Xue, and E. Kaxiras, J. Chem. Phys. **134**, 194706 (2011).
[66] M. Gorgoi, W. Michaelis, T. U. Kampen, D. Schlettwein, and D. R. T. Zahn, Appl. Surf. Sci. **234**, 138 (2004).
[67] D. A. Smith and M. E. Mura, J. Phys. Chem. **98**, 6903 (1994).
[68] Y.-Z. Lan, H.-L. Kang, and T. Niu, Int. J. Quantum Chem. **113**, 949 (2013).
[69] Y. J. Zheng, Y. L. Huang, Y. F. Chen, W. J. Zhao, G. Eda, C. D. Spataru, W. J. Zhang, Y. H. Chang, L. J. Li, D. Z. Chi, S. Y. Quek, and A. T. S. Wee, ACS Nano **10**, 2476 (2016).
[70] D. A. Egger, Z. F. Liu, J. B. Neaton, and L. Kronik, Nano Lett. **15**, 2448 (2015).